doi:10.1093/jmcb/mjab032
Published online May 28, 2021

Article

Three-dimensional ATUM-SEM reconstruction and analysis of hepatic endoplasmic reticulum–organelle interactions

Yi Jiang [1,2,†], Linlin Li[1,†], Xi Chen[1], Jiazheng Liu[1,3], Jingbin Yuan[1,2], Qiwei Xie[4], and Hua Han[1,3,5,*]

[1] National Laboratory of Pattern Recognition, Institute of Automation, Chinese Academy of Sciences, Beijing 100190, China
[2] School of Artificial Intelligence, University of Chinese Academy of Sciences, Beijing 101408, China
[3] School of Future Technology, University of Chinese Academy of Sciences, Beijing 101408, China
[4] Data Mining Lab, Beijing University of Technology, Beijing 100124, China
[5] CAS Center for Excellence in Brain Science and Intelligence Technology, Shanghai 200031, China
[†] These authors contributed equally to this work.
* Correspondence to: Hua Han, E-mail: hua.han@ia.ac.cn

Edited by Xuebiao Yao

The endoplasmic reticulum (ER) is a contiguous and complicated membrane network in eukaryotic cells, and membrane contact sites (MCSs) between the ER and other organelles perform vital cellular functions, including lipid homeostasis, metabolite exchange, calcium level regulation, and organelle division. Here, we establish a whole pipeline to reconstruct all ER, mitochondria, lipid droplets, lysosomes, peroxisomes, and nuclei by automated tape-collecting ultramicrotome scanning electron microscopy and deep learning techniques, which generates an unprecedented 3D model for mapping liver samples. Furthermore, the morphology of various organelles and the MCSs between the ER and other organelles are systematically analyzed. We found that the ER presents with predominantly flat cisternae and is knitted tightly all throughout the intracellular space and around other organelles. In addition, the ER has a smaller volume-to-membrane surface area ratio than other organelles, which suggests that the ER could be more suited for functions that require a large membrane surface area. Our data also indicate that ER–mitochondria contacts are particularly abundant, especially for branched mitochondria. Our study provides 3D reconstructions of various organelles in liver samples together with important fundamental information for biochemical and functional studies in the liver.

Keywords: 3D reconstruction, ATUM-SEM, deep learning, liver, ER, MCSs

Introduction

In all eukaryotes, the endoplasmic reticulum (ER) is a contiguous and complicated membrane network, which is formed by interconnected cisternae and tubules with a single lumen (Baumann and Walz, 2001). The ER extends throughout the cell with a high surface area. In the 1950s, the ER was first identified by observing mouse fibroblasts with electron microscopy (EM) (Porter et al., 1945). The ER is composed of rough ER (ribosome rich) and smooth ER (ribosome free), which are generally organized in cisternae or tubular networks, respectively. The polymorphic structure of the ER is intimately related to its functions, including lipid homeostasis, drug metabolism, secretory protein biogenesis, and regulation of Ca^{2+} dynamics (Baumann and Walz, 2001).

The contacts between the ER and other organelles were recognized many years ago (Porter and Palade, 1957; Rosenbluth, 1962; Csordás et al., 2006). What remained unclear was whether the contacts represented short-term interplay or long-term tethering. For example, membrane contact sites (MCSs) were defined as membrane appositions where the distance between two membrane bilayers was $\leq$30 nm (Levine and Loewen, 2006; Helle et al., 2013). The contact is distinguished from vesicle transport and membrane fusion, which are vital for lipid exchange between organelles (Stefan et al., 2017). Subsequent studies focused

Received November 30, 2020. Revised February 16, 2021. Accepted February 24, 2021.

on the forming factors of MCSs and how they regulate communications between the ER and other organelles (De Brito and Scorrano, 2008; Lebiedzinska et al., 2009; Phillips and Voeltz, 2016).

With rapid development of EM technology, its application in biology has also become widespread (Denk and Horstmann, 2004; Knott et al., 2008; Briggman and Bock, 2012). EM displays the ultrastructure of a region of interest with high resolution (nanometer scale). Furthermore, through three-dimensional (3D) reconstruction, we can observe the real 3D structure in the cell. Due to the limitation of low resolution of fluorescence microscopy, the 3D ultrastructure reconstruction of various organelles through EM has become particularly important in the field of biology.

In recent years, the application of deep learning technology to biological study has been increasingly investigated (Xiao et al., 2018; Liu et al., 2020). For example, image processing technology was applied to the contour segmentation of fluorescent protein and EM images. Many previous studies mainly used manual or semimanual methods to obtain the desired 3D reconstruction of the ER and other cell structures with small-scale EM data (Wu et al., 2017). To our knowledge, few studies utilized deep learning technology for 3D reconstruction of the ER and other organelles with large-scale EM data.

The liver is one of the most important models for studying the functions of ER–organelle interactions. Here, we initially used automated tape-collecting ultramicrotome scanning electron microscopy (ATUM-SEM) (Briggman and Bock, 2012) to image liver samples. Then, to map 3D structure of organelles and their connections within the liver tissue, we applied deep learning technology to effectively reconstruct all ER, mitochondria, lipid droplets, lysosomes, peroxisomes, and nuclei. Finally, a systematic analysis of the morphology and interactions between the ER and other organelles was presented, which can provide important basic information for biochemical and functional studies (Figure 1).

Results

We acquired a 3D EM dataset from the liver of an adult C57/BL male mouse by using ATUM-SEM (dataset size: $81.9 \times 81.9 \times 31.5\ \mu m^3$, voxel size: $\pm 5 \times 5 \times 45\ nm^3$). For 3D reconstruction (Figure 2), we first adopted a coarse-to-fine strategy to 3D-align the serial images, and then we obtained a 3D image stack of interest (size: $20 \times 20 \times 31.5\ \mu m^3$) (Figure 2A; Supplementary Video S1, https://www.micro-visions.org/pub/JiangYi/). Afterwards, we designed an image segmentation method based on deep learning to automatically segment various organelles followed by manual proofreading (see Materials and methods; Supplementary Figures S1 and S2). Then, we employed a 3D connection method to calculate the relationship between organelles in 3D (except for the ER, each organelle is represented by a unique label). We reconstructed all ER, mitochondria, lipid droplets, lysosomes, peroxisomes, and nuclei (the Golgi complex was not reconstructed) to generate a 3D model that mapped the liver samples (Figure 2A, the number of organelles reconstructed is 3500 for mitochondria, 224 for lipid droplets, 90 for lysosomes, 4035 for peroxisomes, and 7 for nuclei). We also visualized 3D structure of the organelles by using Amira software (Figure 2B). Furthermore, the morphology and MCSs were systematically analyzed from the 3D model. In Figure 2B (Supplementary Video S2, https://www.micro-visions.org/pub/JiangYi/), the fine 3D structure of the ER and other organelles can be observed clearly at the nanoscale, thus minimizing the reliance on techniques that image at low resolution, such as fluorescence imaging, for our potential understanding of these organelles. In addition, the position relationship between the ER and other organelles can also be observed, which provides accurate evidence of whether MCSs are formed between the ER and other organelles.

A detailed 3D EM structure of the ER and organelles

The 3D EM reconstruction of the liver cell revealed some information about the structure of the ER. For example, the ER is a contiguous and complicated network that is knitted tightly all over the intracellular space and around other organelles (Figure 2B; Supplementary Video S2, https://www.micro-visions.org/pub/JiangYi/). Additionally, local morphology of the ER is also diverse. For instance, according to the 3D structure, the ER next to the nucleus consists of flat cisternae (Figure 3A), and some fenestra are observed in the flat ER from the 0° or 180° viewing direction. Most of the fenestrated, flat ER presents with a dense and side-by-side distribution. In addition, local segments of the ER are not independent but branch out and are interlaced with each other (Figure 3B). We found that the flat cisternae-shaped ER exhibits high membrane curvature only at the edge and is wider than the middle section of the lumen (Figure 3C, white arrow).

As depicted in Figure 3D, the volume of a single lipid droplet is large, and the volume of a single peroxisome is the smallest. In addition, mitochondria present with an irregular shape on direct visual inspection. To measure the volume ratios of organelles in the whole tissue (Figure 3E), the nucleus was also reconstructed in the image stack. Obviously, the cytoplasm (grey) contributes the largest part of the volume. Among the reconstructed organelles, the total volume of mitochondria is the largest. These results indirectly indicate that the energy supply from mitochondria is essential for liver cells. Surprisingly, although the ER is dense and consists of numerous segments (Supplementary Video S2, https://www.micro-visions.org/pub/JiangYi/), the volume occupied by the ER is only 3.25%. Because the double membranes of the ER are close together, a narrow lumen is formed. In addition, lipid droplets and lysosomes are relatively uncommon.

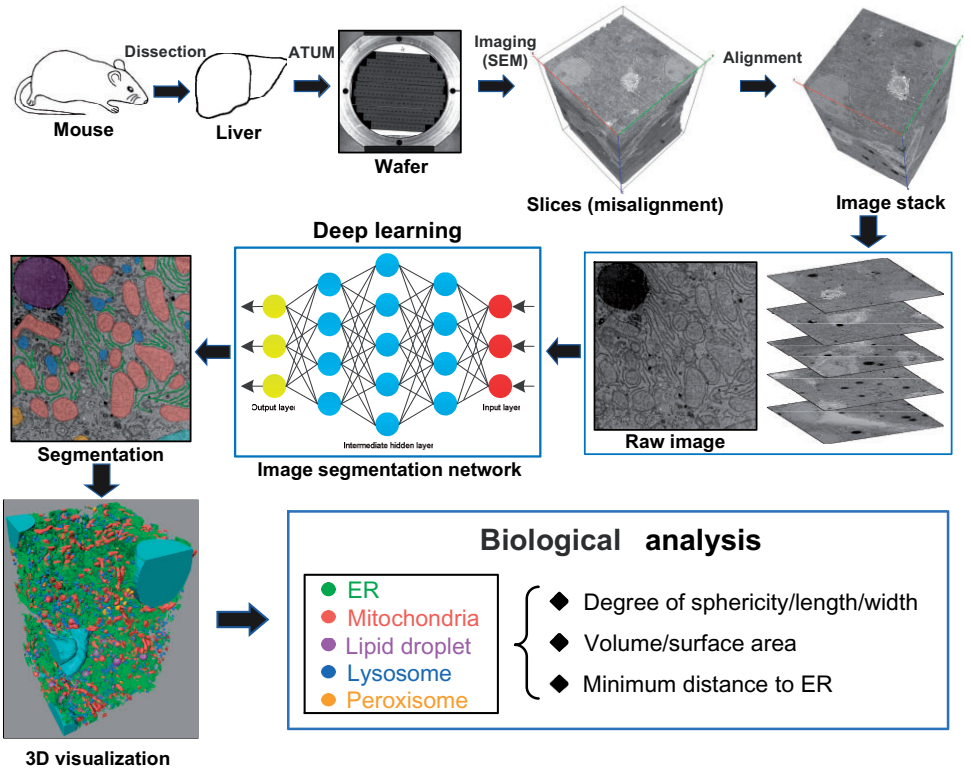

Figure 1 The pipeline of 3D reconstruction and analysis for the mouse liver is based on ATUM-SEM and deep learning technology. The first row (left to right): first, the liver of an adult C57/BL male mouse was dissected, fixed, and embedded. Then, serial sections of liver samples were continuously cut with the ATUM and collected on the tape that was segmented and attached to silicon wafers. Next, serial sections were imaged by SEM to generate serial images (misalignment), and a coarse-to-fine alignment method was adopted to obtain a 3D image stack. The second row (right to left): all raw 2D EM images were input into the image segmentation network to obtain the segmentation images for various organelles. The third row (left to right): 3D visualization provided by Amira software, followed by biological analysis of various organelles based on their 3D reconstructions. Image segmentation network is a simplified diagram and detailed in Supplementary material (Supplementary Figure S1).

As seen from Figure 3D, lipid droplets, lysosomes, and peroxisomes are approximately spherical, so their sphericity was measured for the entire volume (Figure 3F). The closer the sphericity is to 1, the more it tends to be a perfect sphere. A total of 224 lipid droplets and 90 lysosomes, as well as 381 randomly selected reconstructed peroxisomes, were measured. The scatter plot shows that most of the lipid droplets and peroxisomes tend to be spherical, while lysosomes tend to be ellipsoidal.

We calculated the volume-to-surface area (V/SA) ratios of all reconstructed organelles based on our 3D reconstruction (Figure 3G). A total of 705 of the 3500 mitochondria were randomly selected for statistical analysis; these mitochondria were intact and did not appear at the boundary of the volume. The data revealed that the V/SA ratios of various organelles are distinguishable. In the liver, the ER presents with a smaller V/SA ratio than the other organelles, which suggests that the ER could be better suited for functions that require a large membrane surface area, whereas mitochondria, lipid droplets, lysosomes, and peroxisomes may be more suitable for functions that need more internal space. For instance, mitochondria require a large amount of internal space to form the complex mitochondrial cristae structure.

Mitochondria are unique organelles in the liver

Previous study has shown that mitochondria play an important role in the homeostasis of carbohydrate, lipid, and protein metabolism in many organisms (McBride et al., 2006). We found that mitochondria are one of the most abundant organelles in the liver, and the morphology of mitochondria in the liver is diverse (Figure 3E). We can divide it into two types in term of the shape, i.e. unbranched mitochondria (Figure 4A) and branched mitochondria (Figure 4B). In addition, it can be observed that the size of the mitochondria is also different from that shown in Supplementary Video S2 (https://www.micro-visions.org/pub/JiangYi/). Branched mitochondria may be related to division and fusion, because mitochondrial

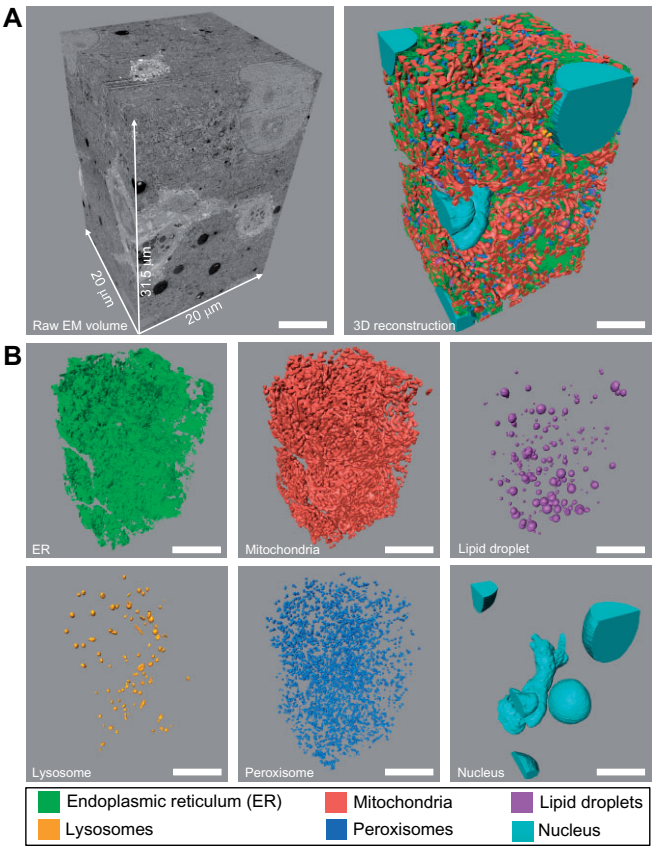

Figure 2 ATUM-SEM volume of mouse liver and 3D reconstruction of various organelles. (**A**) Raw ATUM-SEM volume of the region of interest from the mouse liver (left), with a corresponding size of approximately $20\,\mu m \times 20\,\mu m \times 31.5\,\mu m$. The 3D reconstruction of various organelles (right) corresponds to the left image. (**B**) 3D reconstructions of all ER, mitochondria, lipid droplet, lysosome, peroxisome, and nuclei, which correspond to **A**. Scale bar, 6 μm in **A** and 10 μm in **B**.

proliferation and division are common phenomena in liver cells. However, we cannot rule out the possibility that branched mitochondria are in original shapes and are not related to division and fusion.

We found that unbranched mitochondria are predominant (Figure 4C). The length of the unbranched mitochondria was then measured in 3D reconstruction, revealing that most ranged from 1000 to 2500 nm (mean = 1761.8 nm). Surprisingly, the longest mitochondria exceeded 9000 nm (Figure 4D). The length-to-width ratio of mitochondria can be used as a reference to judge abnormalities. Our results show that this ratio is generally <3 (mean = 2.07), and very few ratios exceed 6 (Figure 4E). After visualization of the spatial relationship between mitochondria and the surrounding ER (Figure 4G and H), we observed that mitochondria are wrapped in the ER, which is a common phenomenon in the liver. This observation was not made by chance, which means that there are crucial connections between mitochondria and the surrounding ER.

MCSs are formed between the ER and mitochondria, lipid droplets, lysosomes, and peroxisomes

Many previous studies have shown that MCSs are essential for the exchange of biological substances between the ER and other organelles. These two membranes contact but do not fuse, delivering substances in the form of nonvesicles. Recently, ER–mitochondria contacts have become a hotspot of research. The ER engages with mitochondria at specialized ER domains known as mitochondria-associated membranes (MAMs), which are indispensable for mitochondrial dynamics and function (Zhou et al., 2020).

Obviously, MCSs between mitochondria and the ER were observed easily when we examined the raw 2D EM images (Figure 5A, left). White arrows indicate the formation of MCSs between mitochondria and the ER. The second to fourth images (Figure 5A) show the 3D reconstruction from different views (XY, XZ, and YZ directions). Meanwhile, we measured the minimum distance between mitochondria and the surrounding ER in 3D reconstruction. According to the sampling survey statistics, we randomly extracted 949 mitochondria from all 3500 reconstructed ones. Figure 5E (red dot on the left) shows the distribution of the minimum distance between the 949 mitochondria and the surrounding ER. Through qualitative observation, the minimum distance between most mitochondria and the ER is within 60 nm. The mean minimum distance was calculated (Figure 5F, the red bar on the left). To determine how many mitochondria and ER formed MCSs (minimum distance ≤30 nm), we computed the percentage of mitochondria that formed MCSs (Figure 5G, the red bar on the left). Approximately 53.7% of the mitochondria and the ER formed MCSs. In addition, we found that branched mitochondria are more likely to form MCSs with ER than unbranched mitochondria (Figure 4F).

When examined in cross-section, ATUM-SEM images show the position of lipid droplets and the surrounding ER. In Figure 5B (left), white arrows indicate the MCSs between lipid droplets and the ER. The second to fourth images (Figure 5B) show 3D reconstruction viewed from different perspectives (XY, XZ, and YZ directions). The distribution of the minimum distance between lipid droplets and the surrounding ER is shown in Figure 5E (purple dot in the middle). The mean minimum distance is 50 nm (Figure 5F, purple bar in the middle). The percentage of lipid droplets that formed MCSs with the surrounding ER was ~29.5% (Figure 5G).

Similarly, we observed the structure of lysosomes and peroxisomes in 2D EM images, with white arrows indicating the MCSs (Figure 5C and D). Likewise, their 3D reconstructions were viewed from different perspectives (XY, XZ, and YZ directions). We found that the minimum distance between lysosomes and the ER is not clustered but similar to a random distribution. However, the minimum distance between most peroxisomes and the ER is <60 nm (Figure 5E). The mean minimum distances between lysosomes and peroxisomes and the ER are 60 and 40 nm, respectively (Figure 5F). Approximately 35.6% of lysosomes and 43.8% of peroxisomes formed MCSs with the ER (Figure 5G).

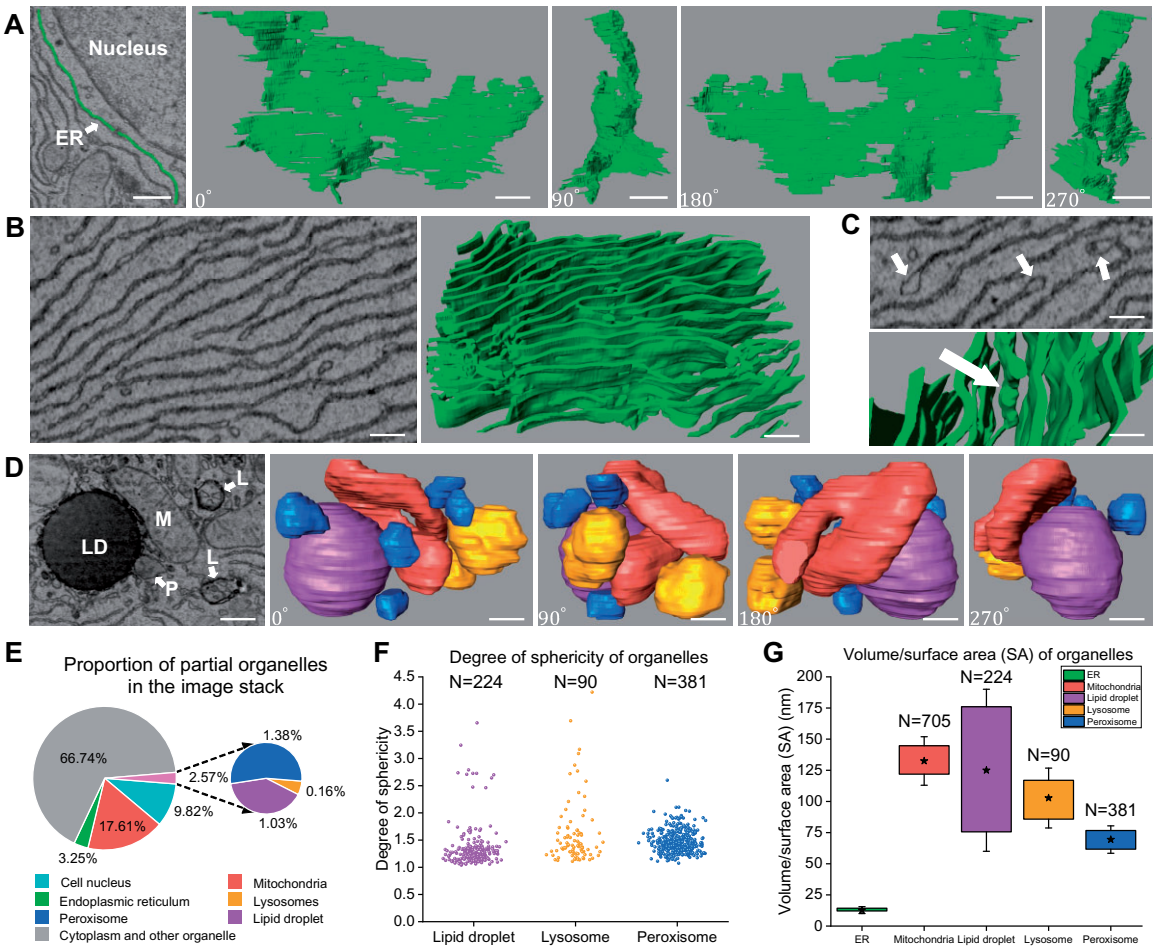

Figure 3 3D ultrastructural analysis of the morphology of the ER and other organelles. (**A**) 3D structure of the ER next to the nucleus. The first image is a raw EM image, and the second to fifth images show the 3D structure from different views (0°, 90°, 180°, 270°, clockwise rotation). (**B**) 3D structure of dense ER area excluding other organelles, branched and interlaced with each other. Left: raw EM image; right: 3D reconstruction. (**C**) The ER presents with high membrane curvature and a wider lumen at the edge (white arrow). Above: raw EM image; below: 3D reconstruction. (**D**) 3D structure of mitochondria, lipid droplets, lysosomes, and peroxisomes (color-coded as in Figure 2). The first image is a raw EM image, and the second to fifth images are 3D reconstructions viewed from different perspectives (0°, 90°, 180°, 270°, clockwise rotation). M, mitochondria; LD, lipid droplet; L, lysosome; P, peroxisome. (**E**) Pie charts show the percentage of reconstructed organelles in the liver tissue, as assessed by inspection of the ATUM-SEM image stack. (**F**) Scatter diagram showing the degree of sphericity of lipid droplets, lysosomes, and peroxisomes, the closer to 1, the closer to the perfect sphere ($N_{\text{lipid droplets}} = 224$, $N_{\text{lysosomes}} = 90$, $N_{\text{peroxisomes}} = 381$ measurements were selected randomly). (**G**) The V/SA ratios were calculated from 3D reconstruction for ER, mitochondria, lipid droplets, lysosomes, and peroxisomes. '★' shows the mean of ratios, and caps show standard error of the mean ($N_{\text{mitochondria}} = 705$ measurements were selected randomly, other as **F**). Scale bar, 750 nm in **A**, 400 nm in **B**, 350 nm in **C**, and 450 nm in **D**.

Discussion

For the first time, we established a whole pipeline to reconstruct the ER and other organelles in the liver by ATUM-SEM (Figure 1), which generated an unprecedented 3D model to map the liver sample. Furthermore, the 3D model allowed a systematic analysis of the distribution and abundance of various organelles and a quantification of the MCSs between the ER and other organelles. In our workflow, ATUM-SEM was adopted to generate image data because it is suitable for large volumes of data, and serial sections can be imaged again when the first imaging fails. In addition, the pixel resolution of ATUM-SEM (x and y directions, 5 nm × 5 nm) was sufficient for recognizing membranes of the ER and other organelles. The main drawback of the ATUM-SEM technique is the low resolution in the z direction (45 nm), which leads to the inability to visualize some tissues. However, for biological structures >100 nm in size, the impact can be ignored. For 3D reconstruction, the ATUM-SEM method requires a more accurate alignment technology to align

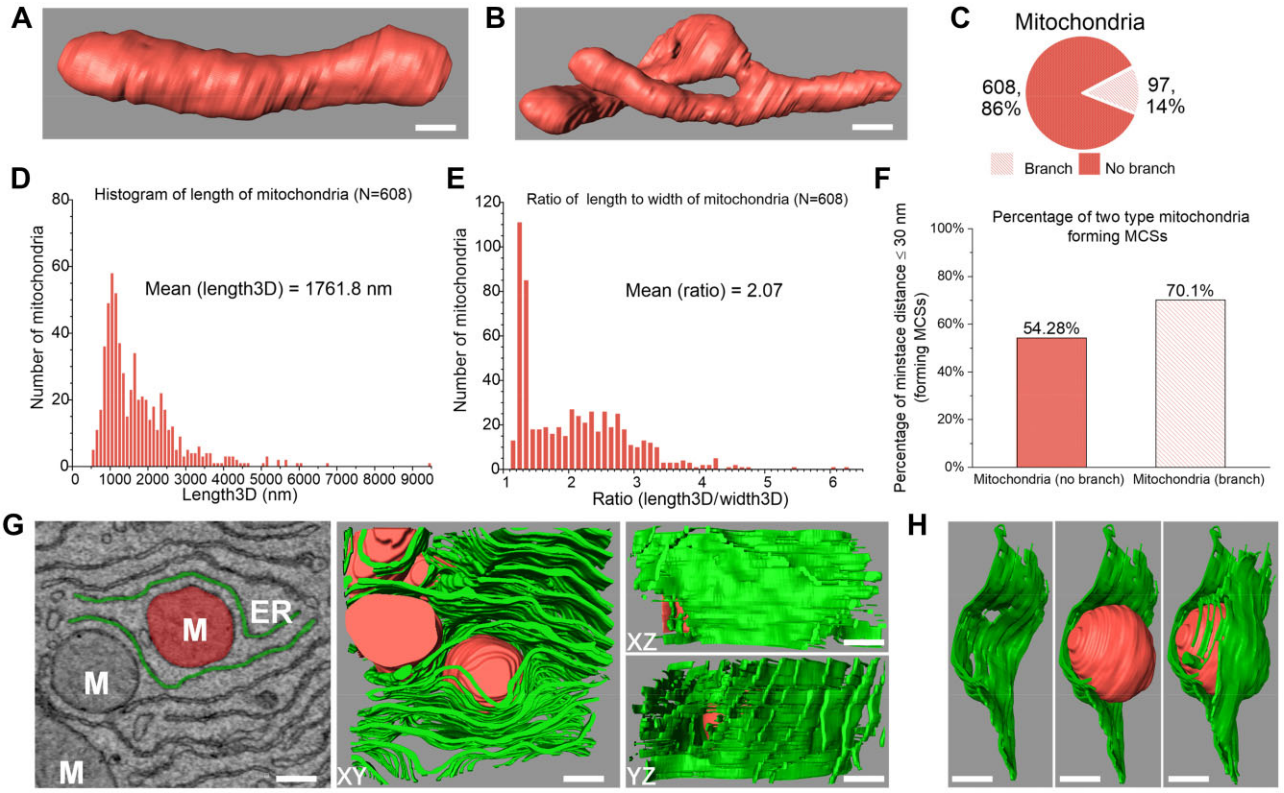

Figure 4 3D structural analysis of mitochondria in the liver. (**A**) Unbranched mitochondria. (**B**) Branched mitochondria. (**C**) Pie chart shows the percentage of unbranched and branched mitochondria (total 705, as in Figure 3G). The shape of all mitochondria is intact. (**D**) The histogram shows the length of unbranched mitochondria in 3D reconstruction, with length3D mean = 1761.8 nm ($N = 608$, as **C**). (**E**) The histogram shows the ratio of length to width of unbranched mitochondria in 3D reconstruction, with ratio mean = 2.07 ($N = 608$, as **C**). (**F**) Bar chart shows the percentage of two types of mitochondria forming MCSs. Percentages are indicated above each graph. (**G**) The spatial relationship between mitochondria and the ER. The first image is a raw EM image, and the other images show the 3D structure from XY, XZ, and YZ perspectives, respectively. (**H**) Mitochondria are surrounded by the ER. Images show the 3D structure from XY, XZ, and YZ perspectives, respectively. Scale bar, 250 nm in **A**, 350 nm in **B**, 190 nm in **G**, and 280 nm in **H**.

the serial images than focused ion beam scanning electron microscopy (FIB-SEM) *in situ* imaging.

To our knowledge, we are the first to apply deep learning technology to automatically segment the ER and other organelles in a 3D EM image stack. Compared with previous semimanual methods, we have a greater advantage in processing large-scale data. For example, the membrane contours of the ER and other organelles were traced semimanually by using 3Dmod software (West et al., 2011, Wu et al., 2017). In addition, our method of segmentation for various organelles is also applicable to FIB-SEM data, provided that the data are reliable. Therefore, our reconstruction workflow can efficiently obtain the 3D structure of various organelles so that biologists can focus more on the study of biological function.

Our 3D model revealed that the ER is distributed densely throughout the tissue to form a continuous membrane network and the local morphology is diverse. We observed that the ER commonly presents with flat cisternae, and the lumen between membrane bilayers is narrow. It was somewhat surprising to us that the fenestrations and edges have a higher membrane curvature than the middle sections in the flat cisternae and that the lumen of the cisterna edges is wider (Figure 3C). As reported previously, reticulons (Rtns) and Yop1 proteins are related to the membrane curvature of the ER, and deletion of these two molecules leads to a loss of cisternal fenestrations (West et al., 2011). We did not perform relevant experiments to confirm the abundance of the two proteins in these regions. Our data are not suitable for reconstructing the tubular ER because it is difficult to distinguish tubular ER and free vesicles in 2D EM images. However, we can observe that the cisternal ER is very dominant in the original EM image stack (Supplementary Video S1, https://www.micro-visions.org/pub/JiangYi/).

The unprecedented 3D model shows spatial distribution and abundance of various organelles (Supplementary Video S2, https://www.micro-visions.org/pub/JiangYi/; Figure 2A and B). In addition to the ER, mitochondria have the tightest distribution and diverse forms. Mitochondria continuously divide and fuse to form a tight network in liver cells. However, the mitochondria are static in our 3D model because they were imaged

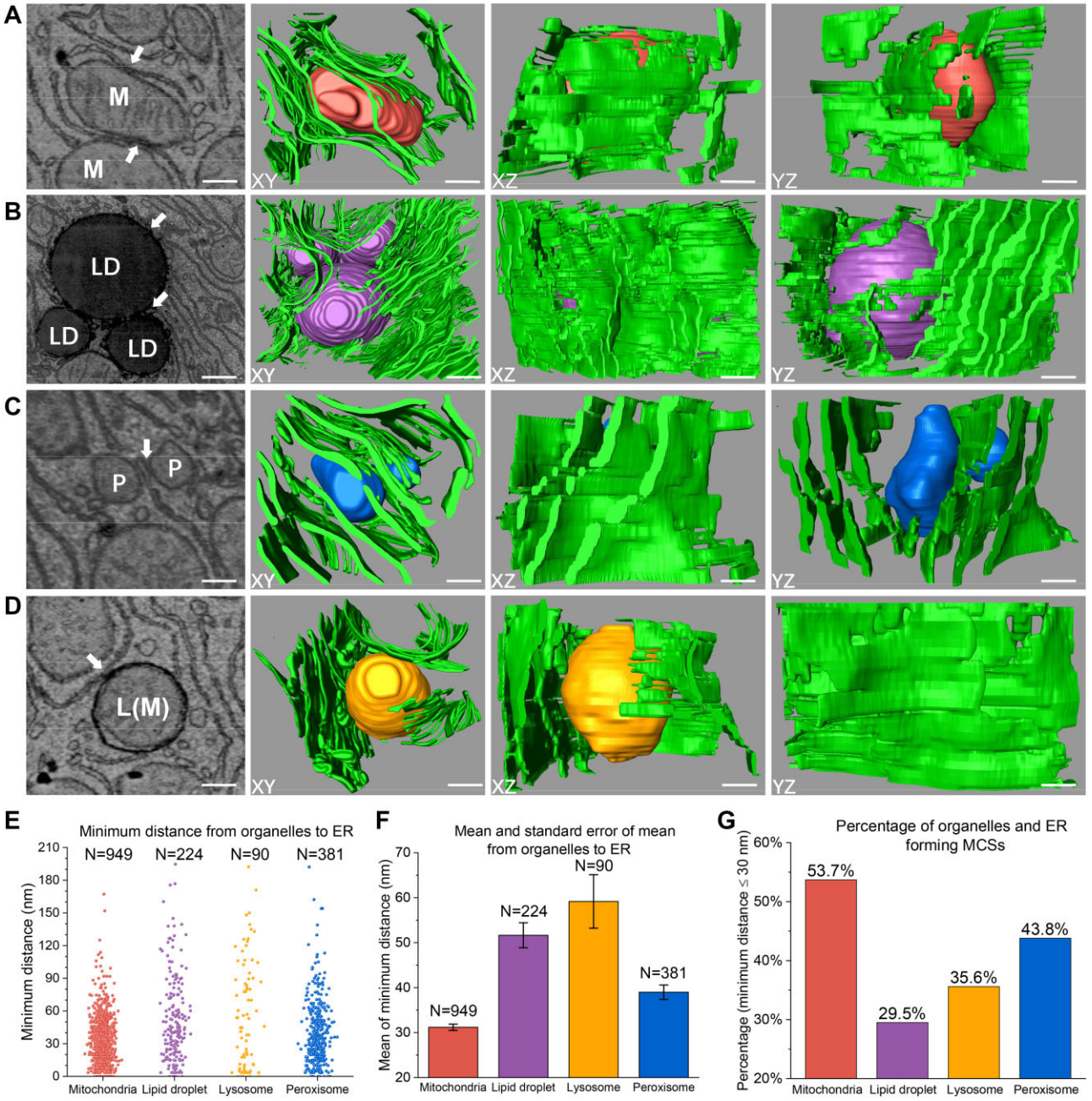

Figure 5 3D analysis of MCSs between the ER and other organelles. (**A**–**D**) MCSs are formed between the ER and mitochondria (**A**), lipid droplets (**B**), lysosomes (**C**), and peroxisomes (**D**). The first image shows the raw EM image, and the white arrow indicates MCSs in a 2D image. The second to fourth images show the 3D reconstruction viewed from different perspectives (XY, XZ, and YZ directions). (**E**) Scatter diagram showing the minimum distance between organelles and the ER. MCSs are formed within 30 nm. $N_{mitochondria} = 949$ measurements, other as Figure 3F. (**F**) Bar chart showing the mean of the minimum distance. The caps show standard error of the mean. (**G**) Bar chart showing the percent of organelles forming MCSs with the ER. Percentages are indicated above each graph. Color-coded as in Figure 2. Scale bar, 290 nm in **A**, 550 nm in **B**, 210 nm in **C**, and 260 nm in **D**.

by EM at a specific moment. Therefore, we cannot ensure whether branched mitochondria are dividing, fusing, or maintaining their original shape. Previous studies have suggested that the abnormal sizes of some mitochondria were related to some liver diseases. For example, giant mitochondria in hepatocytes were related to alcoholic liver disease (Bruguera et al., 1977).

In recent years, the connection between the ER and other organelles has been studied extensively in eukaryotic cells. Increasing number of researchers have realized the

importance of MCSs in cell physiology. Universally, MCSs are studied by fluorescence images or 2D ultrastructures. Here, we used ATUM-SEM to generate a 3D model to analyze the relationship between the ER and other organelles. Due to the static imaging of EM, we should be cautious about the findings that we observe from the 3D structure. However, most cells in the liver should have common features, so our results can provide basic information for biochemical and functional studies of MCSs.

Although the ER and mitochondria play different roles in cells, their interaction is necessary for the exchange of calcium, lipids, and metabolites (Flis and Daum, 2013). Many previous studies have focused on the MCSs between the ER and mitochondria, which are defined as MAMs. Here, we found that more than half of mitochondria formed MAMs with the ER from 3D reconstruction. Moreover, branched mitochondria are more likely to form MAMs with the ER than unbranched mitochondria. Remarkably, branched mitochondria may be in the process of division, and previous studies have indicated that ER–mitochondria contacts coordinate mtDNA replication with mitochondrial division in yeast and human cells (Murley et al., 2013; Lewis et al., 2016). Additionally, a previous study showed that obesity can lead to a marked reorganization of MAMs resulting in mitochondrial calcium overload in the liver, compromising mitochondrial oxidative capacity and augmenting oxidative stress (Arruda et al., 2014).

Lipid droplets are storage organelles for neutral lipids (Wu et al., 2018). Contacts between the ER and lipid droplets are frequent and conspicuous. However, our data show that the lipid droplet is not enfolded by the ER; instead, the edge of the ER is in contact and displays continuity with the lipid droplet membrane, displaying the continuity of the membrane (Figure 5C). These contacts have been defined as membrane bridges, which are closely related to the unique structure and biological process of lipid droplets.

Lysosomes are essential organelles in the cell that can decompose substances that enter the cell from the outside world and digest the local cytoplasm and organelles of the cell itself. Recent study has shown that ER–lysosome contacts are signaling hubs that enable cholesterol sensing by mTORC1, and targeting the sterol-transfering activity of these signaling hubs could be beneficial in patients with Niemann–Pick disease, type C (Lim et al., 2019). Our data show that the lysosome is in low density and can take on a variety of shapes, such as spherical, ellipsoidal, and elongated. In addition, we observed that lysosomes dissolve mitochondria and peroxisomes. Furthermore, the MCSs between the ER and lysosomes are also indispensable to the physiological function of cells.

Peroxisomes are ubiquitous organelles in cells. The peroxisome plays a crucial role in metabolism, and many of these metabolic functions are carried out in partnership with the ER (Wu et al., 2018). In addition to the ER, peroxisomes are intimately associated with mitochondria and lipid droplets, and their ability to carry out fatty acid oxidation and lipid synthesis, especially the production of ether lipids, may be critical for generating cellular signals required for normal physiology (Lodhi and Semenkovich, 2014). However, peroxisomes have received little attention due to their small size. Our data show that peroxisomes are the smallest organelles in our reconstructed image stack but are omnipresent (Supplementary Video S2, https://www.micro-visions.org/pub/JiangYi/; Figure 2B). Like lipid droplets, peroxisomes are also considered to be derived from the ER. Contacts between peroxisomes and the ER are also frequent (Figure 5D).

In summary, our results enhance the knowledge about 3D structure, distribution, and abundance of various organelles in liver cells. They also enable us to determine the MCSs between the ER and other organelles at a nanometer resolution. However, these results only present qualitative and quantitative information from a structural perspective based on static imaging. Therefore, our findings require further EM and dynamic imaging to verify their uniqueness, including whether the MCSs between the ER and other organelles represent short-term interplay or long-term tethering and whether the same phenomenon occurs in other tissues of the liver. Notably, MCSs are known to be linked to liver diseases. The ablation of Mfn2 in the liver revealed that the destruction of ER–mitochondria phosphatidylserine transfer is one mechanism involved in the development of liver disease (Hernández-Alvarez et al., 2019).

Materials and methods

Animals

An adult C57/BL male mouse was kept in a temperature-controlled room with a 12-h light–dark cycle, and was fed with standard mouse chow and normal water. All animal care procedures and research were approved by the Institutional Animal Care and Use Committee of Chinese Academy of Science.

Fixation of mouse liver tissue

The mouse liver tissues were immersed in 4% (*w*/*v*) paraformaldehyde and 2.5% glutaraldehyde (Sigma, G5886). Then, the samples were fixed in 2% OsO_4 (Ted Pella, 18451) in phosphate buffer (0.1 M, pH 7.4) for 90 min at room temperature. The staining buffer was replaced with 2.5% ferrocyanide (Sigma, 234125) in phosphate buffer (0.1 M, pH 7.4) for another 90 min at room temperature. The samples were washed three times with 0.1 M phosphate buffer and incubated with filtered thiocarbohydrazide (TCH, Sigma, 223220) for 45 min at 40°C. Next, the samples were fixed again with unbuffered 2% OsO_4 for 90 min and then incubated overnight in 1% uranyl acetate aqueous solution at 4°C. After incubated with a lead aspartate solution [0.033 g lead nitrate (Sigma, 228621) dissolved in 5 ml 0.03 M aspartic acid (Sigma, 11189, pH 5.0)] for 120 min at 50°C, the samples were dehydrated through a gradient ethanol series (50%, 70%, 80%, 90%, and 100% ethanol, 10 min each) and pure acetone. Finally, the samples were embedded with Epon 812 resin (SPI, 02660-AB).

ATUM-SEM imaging

Serial sections of liver samples were continuously cut through a commercial ATUM with a diamond knife (Diatome, MC16425) and collected on Kapton polyimide tape (width 8 mm, thickness 100 μm). Then, the tape was segmented and attached to 4-inch silicon wafers by a double-coated carbon conductive tape (Ted Pella). Next, the wafers were coated with 6 nm of carbon via a high-vacuum film deposition instrument (Leica) to avoid charging. Eventually, serial sections were imaged by SEM (Zeiss Gemini 300) with a resolution of 5 nm/pixel and a dwell time of 2–5 μs.

Image alignment

After the serial image dataset was acquired through SEM, all images were inspected manually. If sections were missed or contaminated during imaging, the sections could be imaged again. Since we adopted the ATUM method and the samples were not imaged *in situ*, nonlinear distortion of the images was inevitable. Therefore, serial image alignment was indispensable in obtaining a 3D EM image stack. In this case, we adopted a coarse-to-fine strategy to align the serial images. First, we performed coarse alignment by extracting corresponding points between adjacent sections with an affine transformation model on the raw serial images (16000 × 16000 pixels). Then, we intercepted the region of interest (6000 × 6000 pixels). Next, we performed fine alignment (Chen et al., 2018), which involves pairwise correspondence extraction between adjacent sections by SIFT flow (Liu et al., 2011), correspondence position adjustment for all sections, and image wrapping by the moving-least-square method (Schaefer et al., 2006). Because the image will contain a small offset to produce black borders after fine alignment, we intercepted the area without the black border (4000 × 4000 pixels) through the entire serial image stack. Thus, we acquired a stack of 702 images (4000 × 4000 pixels), with a corresponding size of approximately 20 μm × 20 μm × 31.5 μm.

Workflow for 3D reconstruction

The workflow for 3D reconstruction of the 3D EM image stack was as follows. We first designed an image segmentation network to automatically segment all ER, mitochondria, lipid droplets, lysosomes, peroxisomes, and nuclei (Supplementary Figure S1). Each raw 2D EM image was input to the deep learning network to obtain the segmentation images for various organelles. The performance of our image segmentation network is presented quantitatively (Dice coefficient: 0.882 for the ER, 0.9797 for mitochondria, 0.9835 for lipid droplets, 0.9213 for lysosomes, 0.9064 for peroxisomes, and 0.9887 for the nucleus; see Supplementary Table S1) and qualitatively (Supplementary Figure S2). Next, we employed a 3D connection method (Li et al., 2018) to calculate the relationship between each organelle in 3D (except for the ER, each organelle is represented by a unique label). For the architecture and implementation details of the image segmentation network, see Supplementary material.

3D visualization and quantification

Amira software (Stalling et al., 2005) was used for 3D visualization of the ER and other organelles. In addition, some morphological measurements of the organelles were obtained through Amira software, such as 3D volume, 3D surface area, 3D length, and sphericity (see Supplementary material). Furthermore, the minimum distance between the ER and other organelles was obtained by measuring the closest distance between their contours in the 3D model.

Supplementary material

Supplementary material is available at *Journal of Molecular Cell Biology* online.

Acknowledgements

We would like to thank Lixin Wei, Hongtu Ma, and their colleagues (Institute of Automation, Chinese Academy of Sciences) for their assistance in electron microscopy. We extend special thanks to Chi Xiao, Weifu Li, and Zhenchen Li for critical reading and editing of the manuscript. We also thank the Core Facilities of Life Science, Peking University for assistance with Amira software work.

Funding

This work was supported by the Special Program of Beijing Municipal Science and Technology Commission (Z18110000 3818001 and Z181100000118002), the Strategic Priority Research Program of Chinese Academy of Science (XDB32030200), and International Partnership of Chinese Academy of Science (153D31KYSB20170059).

Conflict of interest: none declared.

Author contributions: Y.J., L.L., Q.X., and H.H. designed the research; Y.J. and L.L. performed the research; L.L. performed ATUM-SEM imaging; X.C. performed the serial image alignment; Y.J. performed 3D reconstruction; Y.J., J.Y., and J.L. performed 3D visualization; Y.J. and L.L. analyzed and interpreted the data; Y.J. wrote the manuscript.

References

Arruda, A.P., Pers, B.M., Parlakgül, G., et al. (2014). Chronic enrichment of hepatic endoplasmic reticulum–mitochondria contact leads to mitochondrial dysfunction in obesity. Nat. Med. *20*, 1427–1435.

Baumann, O., and Walz, B. (2001). Endoplasmic reticulum of animal cells and its organization into structural and functional domains. Int. Rev. Cytol. *205*, 149–214.

Briggman, K.L., and Bock, D.D. (2012). Volume electron microscopy for neuronal circuit reconstruction. Curr. Opin. Neurobiol. *22*, 154–161.

Bruguera, M., Bertran, A., Bombi, J.A., et al. (1977). Giant mitochondria in hepatocytes: a diagnostic hint for alcoholic liver disease. Gastroenterology *73*, 1383–1387.

Chen, X., Xie, Q., Shen, L., et al. (2018). 'Morphology-retained non-linear image registration of serial electron microscopy sections'. In: 2018 IEEE International Conference on Image Processing, Athens, Greece. 3833–3837. Piscataway, USA: IEEE Signal Processing Society.

Csordás, G., Renken, C., Várnai, P., et al. (2006). Structural and functional features and significance of the physical linkage between ER and mitochondria. J. Cell Biol. *174*, 915–921.

De Brito, O.M., and Scorrano, L. (2008). Mitofusin 2 tethers endoplasmic reticulum to mitochondria. Nature *456*, 605–610.

Denk, W., and Horstmann, H. (2004). Serial block-face scanning electron microscopy to reconstruct three-dimensional tissue nanostructure. PLoS Biol. *2*, e329.

Flis, V.V., and Daum, G. (2013). Lipid transport between the endoplasmic reticulum and mitochondria. Cold Spring Harb. Perspect. Biol. *5*, a013235.

Helle, S.C., Kanfer, G., Kolar, K., et al. (2013). Organization and function of membrane contact sites. Biochim. Biophys. Acta Mol. Cell Res. *1833*, 2526–2541.

Hernández-Alvarez, M.I., Sebastián, D., Vives, S., et al. (2019). Deficient endoplasmic reticulum-mitochondrial phosphatidylserine transfer causes liver disease. Cell *177*, 881–895.

Knott, G., Marchman, H., Wall, D., et al. (2008). Serial section scanning electron microscopy of adult brain tissue using focused ion beam milling. J. Neurosci. *28*, 2959–2964.

Lebiedzinska, M., Szabadkai, G., Jones, A.W., et al. (2009). Interactions between the endoplasmic reticulum, mitochondria, plasma membrane and other subcellular organelles. Int. J. Biochem. Cell Biol. *41*, 1805–1816.

Levine, T., and Loewen, C. (2006). Inter-organelle membrane contact sites: through a glass, darkly. Curr. Opin. Cell Biol. *18*, 371–378.

Lewis, S.C., Uchiyama, L.F., and Nunnari, J. (2016). ER–mitochondria contacts couple mtDNA synthesis with mitochondrial division in human cells. Science *353*, aaf5549.

Li, W., Liu, J., Xiao, C., et al. (2018). A fast forward 3D connection algorithm for mitochondria and synapse segmentations from serial EM images. BioData Min. *11*, 24.

Lim, C.Y., Davis, O.B., Shin, H.R., et al. (2019). ER–lysosome contacts enable cholesterol sensing by mTORC1 and drive aberrant growth signalling in Niemann–Pick type C. Nat. Cell Biol. *21*, 1206–1218.

Liu, C., Yuen, J., and Torralba, A. (2011). SIFT flow: dense correspondence across scenes and its applications. IEEE Trans. Pattern Anal. Mach. Intell. *33*, 978–994.

Liu, J., Li, L., Yang, Y., et al. (2020). Automatic reconstruction of mitochondria and endoplasmic reticulum in electron microscopy volumes by deep learning. Front. Neurosci. *14*, 599.

Lodhi, I.J., and Semenkovich, C.F. (2014). Peroxisomes: a nexus for lipid metabolism and cellular signaling. Cell Metab. *19*, 380–392.

McBride, H.M., Neuspiel, M., and Wasiak, S. (2006). Mitochondria: more than just a powerhouse. Curr. Biol. *16*, R551–R560.

Murley, A., Lackner, L.L., Osman, C., et al. (2013). ER-associated mitochondrial division links the distribution of mitochondria and mitochondrial DNA in yeast. eLife *2*, e00422.

Phillips, M.J., and Voeltz, G.K. (2016). Structure and function of ER membrane contact sites with other organelles. Nat. Rev. Mol. Cell Biol. *17*, 69–82.

Porter, K.R., and Palade, G.E. (1957). Studies on the endoplasmic reticulum: III. Its form and distribution in striated muscle cells. J. Biophys. Biochem. Cytol. *3*, 269–300.

Porter, K.R., Claude, A., and Fullam, E.F. (1945). A study of tissue culture cells by electron microscopy: methods and preliminary observations. J. Exp. Med. *81*, 233–246.

Rosenbluth, J. (1962). Subsurface cisterns and their relationship to the neuronal plasma membrane. J. Cell Biol. *13*, 405–421.

Schaefer, S., McPhail, T., and Warren, J. (2006). 'Image deformation using Moving Least Squares'. In: ACM SIGGRAPH 2006 Papers (SIGGRAPH '06). 533–540. New York, USA: Association for Computing Machinery.

Stalling, D., Westerhoff, M., and Hege, H.-C. (2005). amira: a highly interactive system for visual data analysis. In: Hansen, C.D., and Johnson, C.R. (eds). The Visualization Handbook. Burlington, USA: Elsevier Butterworth-Heinemann, 749–767.

Stefan, C.J., Trimble, W.S., Grinstein, S., et al. (2017). Membrane dynamics and organelle biogenesis—lipid pipelines and vesicular carriers. BMC Biol. *15*, 102.

West, M., Zurek, N., Hoenger, A., et al. (2011). A 3D analysis of yeast ER structure reveals how ER domains are organized by membrane curvature. J. Cell Biol. *193*, 333–346.

Wu, H., Carvalho, P., and Voeltz, G.K. (2018). Here, there, and everywhere: the importance of ER membrane contact sites. Science *361*, eaan5835.

Wu, Y., Whiteus, C., Xu, C.S., et al. (2017). Contacts between the endoplasmic reticulum and other membranes in neurons. Proc. Natl Acad. Sci. USA *114*, E4859–E4867.

Xiao, C., Chen, X., Li, W., et al. (2018). Automatic mitochondria segmentation for EM data using a 3D supervised convolutional network. Front. Neuroanat. *12*, 92.

Zhou, Z., Torres, M., Sha, H., et al. (2020). Endoplasmic reticulum-associated degradation regulates mitochondrial dynamics in brown adipocytes. Science *368*, 54–60.